Modeling and Measuring UV Cure Kinetics of Thick Dimethacrylate Samples

Yuemei Zhang,[†] David E. Kranbuehl,*[,†] Henry Sautereau,[‡] Gerard Seytre,[‡] and Jerome Dupuy[‡]

Department of Chemistry and Applied Science, College of William and Mary, Williamsburg, Virginia 23187, and Université de Lyon, France; Université Lyon 1, IMP/LMPB Laboratoire des Matériaux Polymères et Biomatériaux; INSA de Lyon, IMP/LMM Laboratoire des Matériaux Macromoléculaires, France; CNRS, UMR5223, Ingénierie des Matériaux Polymères, Villeurbanne F-69621, France

Received August 25, 2008; Revised Manuscript Received November 11, 2008

ABSTRACT: The UV cure kinetics of thick samples composed of a dimethacrylate oligomer, a photobleaching initiator, and in the presence of oxygen are modeled and measured. First, the temporal and spatial variation of initiator concentration and the resulting variation of intensity with depth are calculated using previous results determined from thin samples. Then cure kinetics at different depths are predicted using a model that accounts for a changing concentration of free and trapped radicals. Thereby, the model includes variation in the extent of unimolecular and bimolecular termination as the reaction proceeds. This is different from the classic steady-state assumption involving only bimolecular termination. The model's calculated results are compared with the experimental results measured by transmitted near-FTIR for a number of thick samples of varying thickness exposed to differing intensities and having differing initiator concentrations. The model's predictions are in good agreement with the experimental results.

1. Introduction

UV cure technology was originally used in thin film application, such as for curing coatings, inks, and adhesives. Because of the outstanding advantages of this technology, its application has expanded quickly from traditional thin films to thick films up to a centimeter, such as dental restorative materials,[1−3] gradient structure materials,[4−11] and stereolithography.[12−14] The UV cure kinetics of thin films have been extensively studied experimentally. But most of the reports on the UV cure kinetics of thick samples are based on theoretical calculations.[15−19] For thick films, Terrones and Pearlstein, Miller et al., O'Brien and Bowman, Ivanov, and Decker have developed mathematic models which predict the temporal and spatial variation of light intensity, initiator concentration, and the resulting initiation rate but which assume a number of ideal conditions.[15−18] Their results show there is an optimum initiator concentration for efficient photopolymerization of thick samples.

However, none of the models reported in these papers considered the effect of oxygen that is usually dissolved in systems and decreases the conversion at the surface. For thin film applications, people usually try to remove oxygen to achieve a fast cure under CO_2 or nitrogen to protect the surface. However, for some thick applications, such as producing a gradient structured material, dissolved oxygen may be preferred to achieve a larger structure gradient through depth.

In earlier thick sample UV reports, the cure rate were either not calculated or calculated using the classic steady-state assumption[20] which is based on a bimolecular termination mechanism. However, a number of results point to the existence of another termination mechanism, unimolecular termination due to the observation of "trapped" radicals.[21−26] The combination of unimolecular and bimolecular termination results in a larger exponential dependence of the reaction rate on the intensity and the concentration of the initiator than the widely used value of 0.5. In addition, here the effect of dissolved oxygen in the system is included in the model. In this report, we use this recently developed model that describes a system involving both unimolecular and bimolecular termination.[27]

Here, the UV cure kinetics of a system composed of an oligomer, ethoxylated (4) Bisphenol-A dimethacrylate (CD540), and a photobleaching photoinitiator bis(2,4,6-trimethybenzoyl)phenylphosphine oxide (Irgacure 819) is studied experimentally using transmitted near-FTIR and using the model's predictions for this system. Expanding on previous reports on thick samples, the bulk cure kinetics is calculated from the average change at each depth. The model's calculated results are compared with the experimental results measured by transmitted near-FTIR for samples of varying thickness, exposed to differing intensities, and having differing initiator concentrations.

The experimental results and the model's predictions are used to provide insight into the factors affecting the cure versus depth, the total cure versus time, and the ability of the model to predict the experimental results.

2. Experimental Section

Materials. As previously reported on the thin films,[27] the photoinitiator bis(2,4,6-trimethybenzoyl)phenylphosphine oxide (Irgacure 819, Ciba) was dissolved in the pure oligomer, ethoxylated (4) Bisphenol-A dimethacrylate (CD540, Sartomer), molecular weight 540 with 100 ppm inhibitor. The system was stirred at room temperature for 1 h under nitrogen. The initiator concentration in the system is 0.05−0.2 wt %. All materials were used as received.

FTIR Analysis. In real-time, near-FTIR measurements, with a FTS 7000 Series FTIR spectrometer (Digilab) at William and Mary and a Bruker 55 FTIR Equinox spectrometer at INSA in Lyon are used to measure the transmitted spectrum of the thin samples. The near-FTIR spectrum monitors the decrease of the absorption peak (6160 cm^{-1}) area of the carbon double bonds of the oligomer during the cure process and thereby provides the conversion vs cure time profiles.[28] The sample was prepared by putting it between two glass slides (transmission of IR >95%, transmission of UV at 365 nm >90%) using glass as a spacer to determine the sample thickness.

* To whom correspondence should be addressed.
[†] College of William and Mary.
[‡] Université de Lyon.

10.1021/ma8019283 CCC: $40.75
Published on Web 12/11/2008

The radiation source (200 W Hg lamp) has a 356−365 nm bandpass filter and is equipped with a water filter to remove the IR radiation's sample heating. A fiber-optic cable guides the light to the sample chamber of the FTIR equipment. The intensity of the exposure is adjusted by changing the distance of the fiber-optic cable from the sample and measurement with a radiometer.

Temperature Measurement. A portable AMC thermocouple thermometer with ports connected to thermocouples located at different depths in the sample monitored the temperatures simultaneously. The AMC thermocouple thermometer recorded a value every 2 s.

3. Model Description

3.1. Spatial and Temporal Variation of Light Intensity and Initiator Concentration. The spatial and temporal variation of light intensity has been previously studied.[6,7,12,15−17,29,30] The monomer absorbs light at the wavelength of the initiator, 366 nm. Since oligomer absorption is negligible compared to the monomer, the equation of Beer−Lambert law can be written as

$$I_t = I_i \times 10^{-b(\varepsilon_i[\mathrm{PI}]_t + \varepsilon_m[\mathrm{M}])} \quad (1)$$

Here b is the light path length of the sample (cm), I_i is the incident intensity to the surface of the thick sample, I_t is the light intensity at the distance of b from the exposure surface, and ε_i, the absorption coefficient of the initiator, is 760 L mol^{-1} cm^{-1} measured using CD540 as the solvent. [PI], mol L^{-1}, is the concentration of photoinitiator. ε_m, the absorption coefficient of the monomer, is 0.0755 L mol^{-1} cm^{-1} as measured.[27,28] [M], mol L^{-1}, is the concentration of monomer.

In some previous reports, absorption of the monomer is disregarded because the extinction coefficient of monomers is usually much smaller than the extinction coefficient of initiators. However, the fraction of monomers in the system is much larger than the initiator and oligomers. Therefore, the absorbance of the monomers may significantly affect the intensity at a given depth. Here the intensity and initiator concentration vs depth are calculated for both situations, and the effect of the monomer absorption is examined.

In addition, the initiator used here, Irgacure 819, is photobleaching. After the exposure starts, the intensity inside the system increases with exposure time due to the degradation of the initiator and no light absorbance in this range by the photoproducts. Therefore, as time passes more light reaches a given depth. The photolysis of aryl phosphine oxides including Irgacure 819 has been studied.[38,39] The initiator undergoes α-breakage to produce a benzoyl−phosphinoyl pair. The optical absorption spectrum of the benzoyl−phosphinoyl radical pair produced by the UV light shows that the absorption at 365 nm is almost zero.

The degradation rate of the initiator can be expressed using the equation

$$-\frac{\mathrm{d}[\mathrm{PI}]}{\mathrm{d}t} = \phi' I_a \quad (2)$$

ϕ' is the quantum yield of the photoinitiator consumption, the mole number of photoinitiator degraded per einstein absorbed. The value of ϕ' for α-cleavage of bis(acyl)phosphine oxides is reported to be 0.5[38] to produce a benzoyl−phosphinoyl radical pair. (Note: ϕ' is different from ϕ, the quantum yield of initiation, the number of radicals which activate propagation formed for each photon absorbed as often defined.[20]) I_a is the absorbed photon number by the photoinitiator in units of einstein s^{-1} L^{-1}.

I_a can be calculated at various depths and times using eq 3 according to Beer−Lambert's law.

$$I_{(n,m)} = \frac{I_i(1 - 10^{-\varepsilon_i b_n \mathrm{PI}(n,m)})}{b_n} \quad (3)$$

where b_n is the depth of the layer n.

Using eqs 2 and 3 and doing the integration for a small time interval, $t_2 - t_1$

$$[\mathrm{PI}]_{(n,m+1)} = [\mathrm{PI}]_{(n,m)} - \frac{\phi' I_i(1 - 10^{-\varepsilon_i b_n \mathrm{PI}(n,m)})}{b_n}(t_{m+1} - t_m) \quad (4)$$

Using these equations, the change of initiator concentration and light intensity vs exposure time m and sample depth b_n for layer n in a thick sample is calculated.

The UV cure kinetics of this system as a thin film has been studied.[27] A model to describe the cure kinetics involving a changing concentration of free radicals undergoing bimolecular termination and trapped radicals undergoing unimolecular termination was developed.[27] The model is based on the observed existence of a spatial and dynamic heterogeneity in these methacrylate systems, a phenomena first predicted by Duzek.[31−33] It is now known that microgel regions are formed near the onset of the reaction and are surrounded by "monomer pools" in which radicals generated therein are highly mobile. The radicals in the growing microgel/macrogel regions have very limited mobility and are considered trapped, approximated as immobile in the model. The existence of a changing percentage of mobile and trapped radicals has been observed by ESR.[34,35] The existence of a dynamic heterogeneity resulting from the growth of the microgel/macrogel regions as the reaction progresses has been observed in frequency-dependent dielectric and mechanical measurements.[36,37] In order to describe the kinetics of this changing heterogeneous system, the difference of two kinetic terms were introduced to describe the changing concentration of mobile radicals. The first term describes the changing total concentration of radicals and the second the changing concentration of trapped radicals. The model assumes a constant rate constant, k_p, as is generally assumed in traditional cross-linking reactions up to reaction quench in the final stage of cure. The existence of both bimolecular and unimolecular termination is accounted for by allowing the exponential dependence of the initiator concentration and the light intensity to be between 0.5 and 1.0, reflecting the existence of both termination reactions.

In our previous paper on this system of dimethacrylate and Irgacure 819, the cure kinetics of thin films were described by eq 5[27]

$$-\frac{\mathrm{d}(\ln([\mathrm{M}(t)])}{\mathrm{d}t} = \left(\frac{I}{32.5}\right)^{0.7}\left(\frac{[\mathrm{PI}]}{0.2}\right)^{0.75} \times \left(\frac{1}{1 + \mathrm{e}^{-30(\alpha-0.05)}} - \frac{1}{1 + \mathrm{e}^{-13.7(\alpha-0.36)}}\right) \quad (5)$$

Here α is the conversion of C═C. The first factor, $1/(1 + \mathrm{e}^{-30(\alpha-0.05)})$, represents the contribution of propagation rate constant k_p times $[\mathrm{M}^\bullet]_{\mathrm{total}}$, the concentration of all radicals in the system. The second factor, $1/(1 + \mathrm{e}^{-13.7(\alpha-0.36)})$, represents the contribution of k_p times $[\mathrm{M}_t^\bullet]$, the concentration of trapped radicals at time t. The coefficients of 30 and 13.7 times the conversion describe the rate of increase in the concentration of total radicals and trapped radicals as the reaction progresses. The numbers 0.05 and 0.36 are the conversion where the total and trapped radical concentration is equal to half of their maximum concentration during the exposure process. The units of I are μW/cm^2, and $[\mathrm{M}_t]$ (mol/L) is the concentration of monomer double bonds in the system at time t.

Thus, after the transmitted light intensity and initiator concentration at a given depth are known, the cure kinetics in a short interval of time at a particular depth in a thick sample can be calculated using eq 5.

Since the system has a certain amount of oxygen dissolved in it, there is an inhibition period before the cure starts. The delay time (the inhibition period) can be calculated using eq 6 based on our previous thin film results on this system.[27]

$$T_d = \frac{5.542}{I \times [\text{PI}]\ \text{wt}\ \% \times 100} \tag{6}$$

A Matlab program is written to perform the calculation by dividing the sample into NL thin layers and dividing the exposure time into m time intervals. Two assumptions are used to simplify the calculation process. First, there is no mass exchange (no diffusion of O_2, CD540, and Irgacure 819) between any two adjacent layers. When the reaction is fast, there is less opportunity for diffusion. In addition, when the light gradient is small, the diffusion is small since the variation of component concentration through depth due to the reaction gradient is small and diffusion is proportional to the difference of component concentrations between two thin layers. Thus, the reaction at each layer can be regarded as a thin sample reaction and studied in a thin film. The second assumption is that the curing at all depths is at room temperature. The increase of temperature due to the exothermal reaction is not considered. It can be significant and will be discussed later for those experiments that have a significant increase in temperature.

All light intensities, $I(x,y)$, and photoinitiator concentrations, PI(x,y), at different depths x and times y are calculated.

According to the original condition, all incident light intensities on the first layer at all times, $I(1,1)$ to $I(1,m)$, are equal to I_i. The incident light intensity that does not change with exposure time as verified by using a radiometer. Then using eq 1, the light intensity through depth before the exposure starts, $I(1,1)$, $I(2,1)$... to $I(n,1)$, can be calculated at time $t(1)$ for all NL layers, 1 through n, using the original concentration values of initiator and monomer.

Then change of initiator concentration versus exposure time of the first thin layer, PI(1,2), PI(1,3)... PI(1,m), can be calculated using eq 4 for each subsequent time interval. Then the transmitted intensity at each subsequent layer at different exposure times, $I(2,2)$, $I(2,3)$... $I(2,m)$, can be calculated using eq 1 as well as the change of initiator concentration versus exposure time using eq 4. Hence, the variation of light intensity and initiator and monomer concentration through depth and exposure time can be calculated, step by step.

The delay times (inhibition periods) of UV cure at each layer at all depths are calculated using eq 6 by substituting I with $I(x,y)$ from step 1 and [PI] with $[\text{PI}]_0$.

The concentration of C═C, $M(x,y)$, and the conversion of C═C, $\alpha(x,y)$, are calculated beginning at the end of this inhibition period as well as α, using eq 7

$$\alpha = 1 - \frac{M}{M_0} \tag{7}$$

$M(x,y)$ is calculated using eq 5 by integration from time $y-1$ to y and substituting $\alpha(x,y-1)$, $I(x,y)$, and PI(x,y).

Finally, the average change of $M(t)$ and $\alpha(t)$ through depth vs exposure time can be calculated by taking the average of all values for each layer at the same exposure time. This result is to be compared with the experimental result measured using real-time transmitted near-FTIR on a series samples with different thicknesses and initiator concentrations.

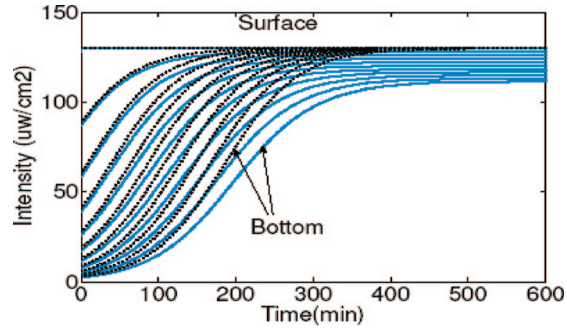

Figure 1. Model predicted intensity at different depths in a thick sample. CD540−0.2 wt % Irgacure 819, $I_i = 130\ \mu\text{W/cm}^2$; thickness of sample is 4 mm, [PI] = 0.2 wt %, $\phi' = 0.5$, NL = 10. (—) Considering the absorption of the monomer, $\varepsilon_i = 760$ L mol^{-1} cm^{-1}, ε_m is 0.0755 L mol^{-1} cm^{-1}; (---) without considering the absorption of the monomer.

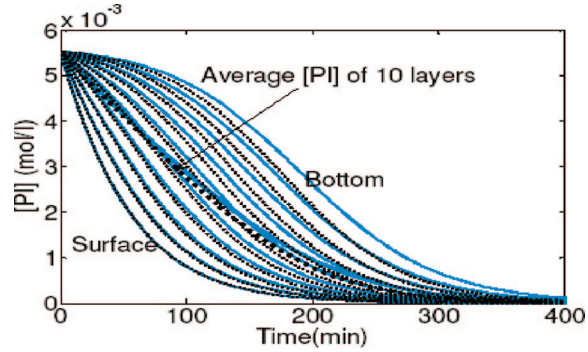

Figure 2. [PI] vs time at different depths in a thick sample. CD540−0.2 wt % Irgacure 819, $I_i = 32.5\ \mu\text{W/cm}^2$, thickness of sample is 4 mm, [PI] = 0.2 wt %, $\phi' = 0.5$, NL = 10. (—) Considering the absorption of monomer, $\varepsilon_i = 760$ L mol^{-1} cm^{-1}, ε_m is 0.0755; (---) without considering the absorption of monomer. Two darker curves in the middle of other curves are the average of all 10 layers.

4. Results and Discussion

4.1. Model Predictions of UV Cure Kinetics of Thick Samples. *Light Intensity and Initiator Concentration versus Exposure Time and Depth in Thick Samples.* Using the model described in section 3, the light intensity and the concentration of initiator are calculated versus exposure time and depth for two situations. The first includes the absorbance of the monomer, and the second does not consider the absorbance of the monomer. Both results are listed together in Figure 1.

Figure 1 shows that when the absorption of the monomer is considered, the transmitted intensity increases slower than the predictions without considering the absorption of the monomer.

The predicted changes in initiator concentration versus exposure time at different depths are shown in Figure 2 for both situations. For both cases, the initiator concentration in every layer decreases with exposure time. At the deeper layers, the dotted curves which neglect monomer absorption decrease faster than the solid curves where monomer absorption is accounted for. Thus, the predicted consumption of [PI] at deeper layers is slower when the absorption of the monomer is considered than when absorption of the monomer is neglected. The deeper the layer (or the thicker the sample), the larger is the difference. Therefore, it is necessary to consider the absorption of the monomer especially when the sample is thick.

Predicted Cure Kinetics vs Depth in Thick Samples under Isothermal Conditions. Using the model described in section 3, the cure kinetics at different depths assuming isothermal conditions is calculated for a FTIR monitored 4 mm thick sample of CD540 with 0.2 wt % Irgacure 819 initiator

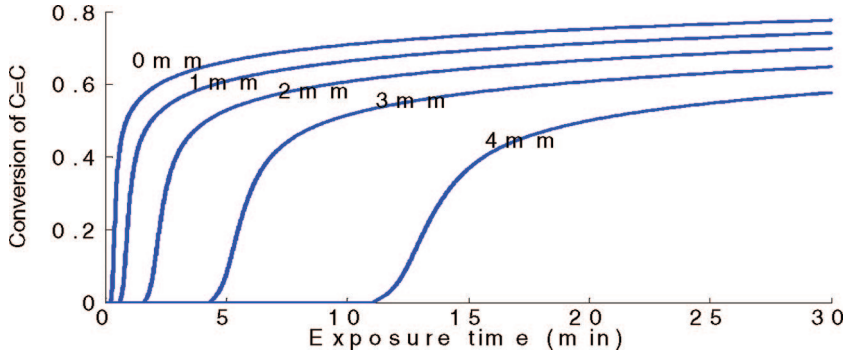

Figure 3. Predicted UV cure kinetics of CD540−0.2 wt % Irgacure 819 at different depths as marked in the figure from 0 to 4 mm. I_i = 130 μW/cm^2, time interval is 0.01 min, layer thickness = 0.05 mm.

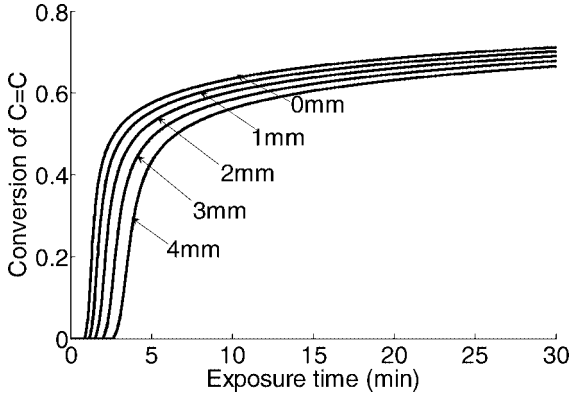

Figure 4. Predicted UV cure kinetics of CD540−0.05 wt % Irgacure 819 at different depths. The depths are marked in the figure as 0−4 mm. I_i = 130 μW/cm^2. Time interval is 0.01 min, layer thickness = 0.05 mm.

concentration, under 130 μW/cm^2 radiation intensity. Using the model, the sample is divided into eighty 0.05 mm thin layers. Using 0.01 min as the time interval, the calculated cure kinetics at the surface, and at 1, 2, 3, and 4 mm depth are shown in Figure 3. From Figure 3, the cure kinetics are strongly dependent on depth. The polymerization at the surface layers is much faster than the reaction at the bottom layers because the intensity decreases significantly with depth, as shown in Figure 1.

Next, the cure kinetics are predicted for another FTIR monitored 4 mm thick CD540 sample but with a lower 0.05 wt % Irgacure 819 initiator under the same radiation conditions. The calculated result is shown in Figure 4. In Figure 4, the cure kinetics is also faster at surface than at the bottom layers. Comparing Figures 3 and 4, the cure at the surface layer is faster for the system with more initiator (Figure 3). However, the cure at the bottom layer is slower for the system with more initiator (Figure 3). The reaction is more homogeneous through depth for the sample with less photoinitiator because the absorption of light with increasing depth is higher for the system with more initiator. In summary, the gradient of intensity vs depth for the sample with 0.2 wt % initiator is more pronounced than the sample with 0.05 wt % initiator, and so is the cure rate.

Predicted Bulk Cure Kinetics in Thick Samples. Using the model predicted cure kinetics at different depths, the bulk cure kinetics is predicted by calculating the average of the conversion of C═C in all layers from the surface to the bottom at the same exposure time. These samples are divided into eighty 0.05 mm thin layers for the 4 mm thick samples. The cure curves at each layer from surface to bottom, and the average cure kinetics are shown in Figure 5. This figure shows that the inhibition period of the bulk cure is determined by the cure near the surface. But the bulk cure rate and the final conversion are affected by the delay time and cure rate which vary with each layer.

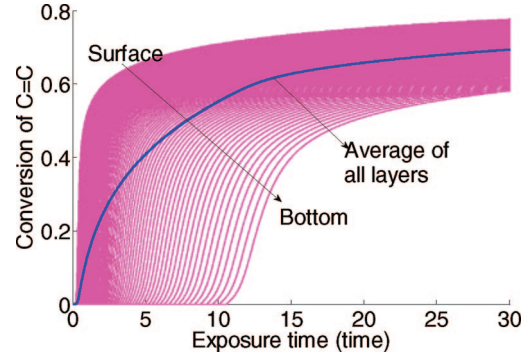

Figure 5. Predicted values using eqs 1−6. Cure kinetics of a 4 mm thick sample, CD540−0.2 wt % Irgacure 819, I_i = 130 μW/cm^2. Time interval is 0.01 min, layer thickness = 0.05 mm. (•••) Cure curves of sample in 0.05 mm thin layers at different depths; (—) average cure curve of all thin layers in thick sample.

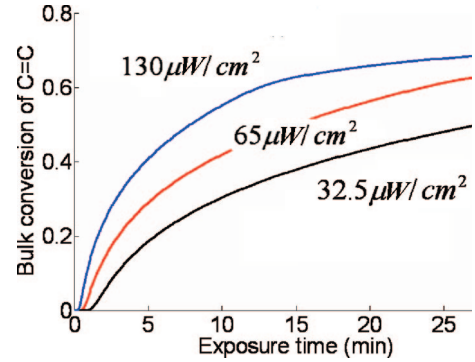

Figure 6. Predicted values using eqs 1−6. Bulk cure kinetics of 4 mm thick sample, CD540−0.2 wt % Irgacure 819 under different radiation intensities. Time interval is 0.01 min, layer thickness = 0.05 mm. Incident radiation intensity is marked in the figure.

Next, the intensity and initiator concentration effects on the bulk cure kinetics are calculated using the same calculation method as in Figure 5. The bulk cure kinetics of 4 mm thick samples of CD540−0.2 wt % Irgacure 819 under different radiation intensities are shown in Figure 6. Figure 6 shows that increasing the light intensity increases the cure rate and decreases the inhibition period of these 4 mm thick samples of CD540 with 0.2 wt % Irgacure 819. This result is similar to that in the previously studied 0.05 mm thin samples.[27]

Then, the initiator concentration effect on the bulk cure kinetics of 4 mm thick samples of CD540−Irgacure 819, with varying initiator concentration, [PI], and under the same radiation intensity is calculated. The results are shown in Figure 7. Figure 7 shows that the inhibition period is shorter for the system with more initiator. Again this is similar to the result

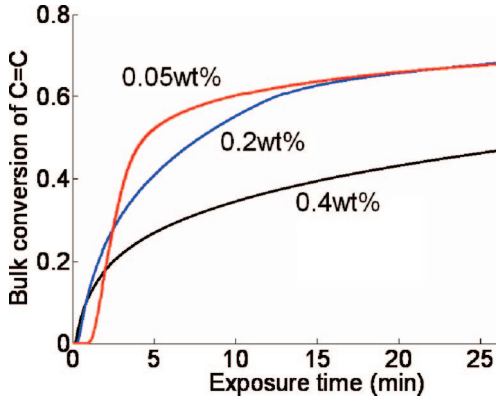

Figure 7. Predicted values using eqs 1−6. Bulk cure kinetics of 4 mm thick sample, CD540−Irgacure 819 with varying initiator concentrations. $I_i = 130\ \mu W/cm^2$. Time interval is 0.01 min, layer thickness = 0.05 mm. Initiator concentration is marked in the figure.

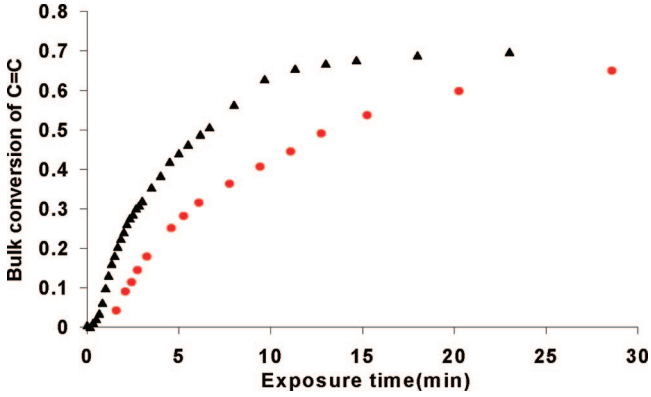

Figure 8. FTIR measured bulk conversion vs time for the cure of 4 mm thick system, CD540−0.2 wt % Irgacure 819. (▲) $I_i = 130\ \mu W/cm^2$; (●) $I_i = 65\ \mu W/cm^2$.

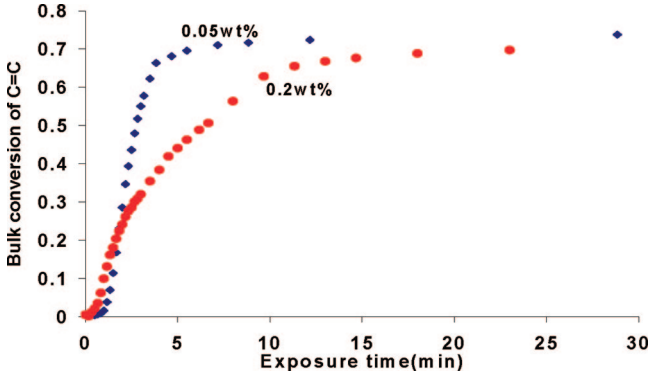

Figure 9. FTIR measured bulk conversion vs time for the cure of 4 mm thick system, CD540−Irgacure 819 under the exposure intensity, $I_i = 130\ \mu W/cm^2$. Initiator concentration are marked in the figure: (◆) [PI] = 0.05 wt %; (●) [PI] = 0.2 wt %.

for 0.05 mm thin samples. However, Figure 7 shows that increasing initiator concentration does not increase the average polymerization rate of the 4 mm thick samples. This is different from the conclusion for thin samples. The reason for the abnormal phenomena is the significant decrease of light intensity through the depth in a thick sample with a higher initiator concentration. A high initiator concentration results in an extremely slow reaction rate at the bottom. Since the bulk cure kinetics is the average of cure in each layer at all depths, the slow reaction rate and long delay time at the bottom decrease the bulk cure rate. But the inhibition period is determined only by the reaction in the layers near the surface (as shown in Figure

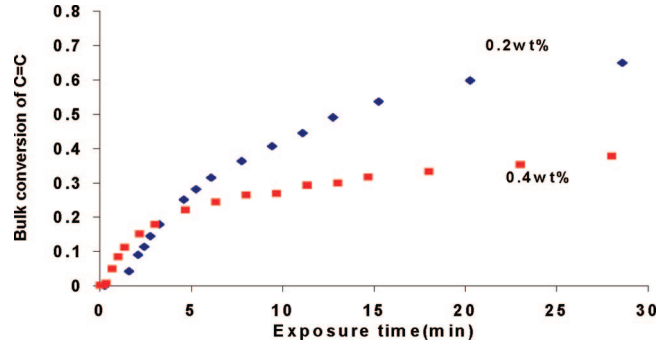

Figure 10. FTIR measured bulk conversion vs time for the cure of 4 mm thick system, CD540−Irgacure 819, under the exposure intensity, $I_i = 65\ \mu W/cm^2$. Initiator concentrations are marked in the figure: (◆) [PI] = 0.2 wt %; (■) [PI] = 0.4 wt %.

5) where the intensity is not significantly decreased but the initiator concentration is higher. So the inhibition period in the surface layers is shorter, as is the inhibition period for the bulk cure.

These results are consistent with previous modeling of the isothermal cure characteristics of thick samples.[15−18] Regardless of the kinetic equations used to model the reaction rate in a thin layer, models divide the thick sample up into a series of thin layers at varying depths. It is well-known that the reaction rate at a given depth depends on the initiator concentration, the molar extinction coefficient of the initiator and of the monomer plus the polymer at the incident radiation frequency, and the intensity of the incident radiation. Our model addresses all of these factors. Our results as do previous results show that if the concentration times the major extinction coefficient of the initiator is large, there is a large gradient in the UV intensity vs depth. Thus, the sample cures from the top down, sometimes referred to as frontal polymerization. The advantage of our model is that the kinetic equation describing the kinetics in each layer vs depth is a more realistic physical representation of the spatial heterogeneity of the sample. That at each depth the sample exhibits regions of high mobility and essentially no mobility. Our model accounts for the decreasing the fraction of space occupied by the mobile regions with time and at each depth.

When the temperature during the reaction is no longer close to isothermal conditions, many more parameters which are generally not only unique for a particular resin but unique to the environment in which the resin is cured are needed.[17] First, the temperature dependence of the effective rate constant times the concentration of trapped radicals vs time must be determined in thin sample measurements for a particular resin. Then an energy balance equation for each depth and time that includes heat generated by the reaction vs depth/time, heat accumulation, and parameters that account for the heat transfer properties at the top and bottom surface of the film are needed. As previously shown, using a variety of possible conditions, the thermal boundary at the interface of the top and bottom surface of the film going from thermally insulating to conductive will have a very large effect.[17] Thus, addressing nonisothermal cure is an exercise which is strongly dependent on a given cure environment.

4.2. Measured UV Cure Kinetics of Thick Samples Using Real-Time Transmitted Near-FTIR. In section 4.1, the cure kinetics of a number of samples of CD540 with Irgacure 819 was predicted using the model described in section 3. In this section, the changing total concentration of C═C of monomer in these thick samples is monitored using real-time transmitted near-FTIR.

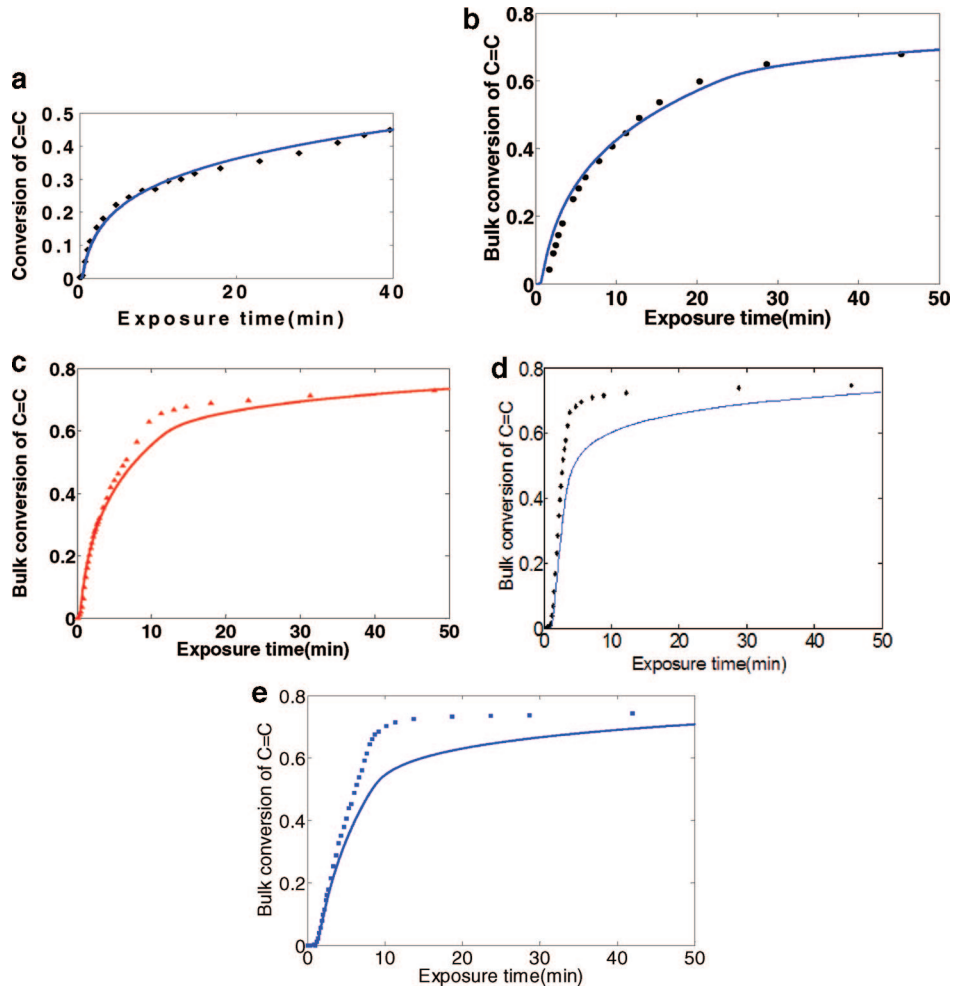

Figure 11. (a) Bulk conversion vs time for the cure of 4 mm thick system, CD540−0.4 wt % Irgacure 819. $I_i = 65\ \mu W/cm^2$. (◆) FTIR measured data; (—) predicted cure curve using eqs 1−6. (b) Bulk conversion vs time for the cure of 4 mm thick system, CD540−0.2 wt % Irgacure 819. $I_i = 65\ \mu W/cm^2$. (●) FTIR measured data; (—) predicted cure curve using eqs 1−6. (c) Bulk conversion vs time for the cure of 4 mm thick system, CD540−0.2 wt % Irgacure 819 at 130 $\mu W/cm^2$ (▲) FTIR measured data; (—) predicted cure curve using eqs 1−6. (d) Bulk conversion vs time for the cure of 4 mm thick system, CD540−0.05 wt % Irgacure 819. $I_i = 130\ \mu W/cm^2$ (◆) FTIR measured data; (—) Predicted cure curve using eqs 1−6. (e) Bulk conversion vs time for the cure of 8 mm thick system, CD540−0.05 wt % Irgacure 819. $I_i = 130\ \mu W/cm^2$. (■) FTIR measured data; (—) predicted cure curve using eqs 1−6.

Table 1. Increase of Temperature in Thick Samples during the Cure under Different Conditions

				maximum increase of temp (°C)	
Figure No.	[PI], wt %	intensity, $\mu W/cm^2$	sample thickness (nm)	surface	bottom third
11a	0.4	65	4	9	4
11b	0.2	65	4	12	10
11c	0.2	130	4	16	13
11d	0.05	130	4	12	20
11e	0.05	130	8	14	25

First, the exposure intensity effect on the cure kinetics is studied experimentally under varying UV intensities. The experimentally measured bulk cure curves of CD540 with 0.2 wt % Irgacure 819 at two different radiation intensities are shown in Figure 8. Increasing radiation intensity increases the bulk cure rate of a 4 mm thick sample. This agrees with the theoretically predicted result in Figure 6.

Second, the initiator concentration effect on the bulk cure kinetics is reported in Figure 9 for the cure of CD540−Irgacure 819 with 0.2 and 0.05 wt % initiator concentration at 130 $\mu W/cm^2$ radiation intensity. Figure 9 shows that increasing initiator concentration results in a shorter inhibition period but a slower cure rate. This matches the predicted result in Figure 7 under the same exposure conditions. The initiator concentration effect on the bulk cure kinetics is also studied at another intensity, 65 $\mu W/cm^2$, for the system of CD540−Irgacure with 0.2 and 0.4 wt % photoinitiator concentration in Figure 10. Thus, both Figures 9 and 10 show that for these 4 mm thick samples of CD540 with Irgacure 819 increasing initiator concentration decreases the bulk cure rate, but it does shorten the inhibition period.

4.3. Comparison of the Predicted UV Cure Curves and Real-Time Transmitted Near-FTIR Results. In Figures 11a−c, the experimental data are plotted together with the corresponding predicted data under the same condition to evaluate the model's predictions. The cure conditions of these comparison Figures are listed in Table 1. The predicted data match the experimental data well in Figures 11a−c where the initiator concentration is higher and the radiation intensity is lower. However, in Figures 11d,e, the predicted data only match the experimental data up to $\alpha = 0.4$. At higher conversions, the experimentally measured conversion is higher than predicted. This is due to the exothermal reaction that results in an increase of temperature in these thick samples during the later stages of the cure. An increase of temperature results in an increase in the reaction rate and the final conversion.

Table 1 reports the maximum temperature measured at the surface and at a depth approximately one-third from the bottom

for the runs with varying initiator concentration, intensity, and thickness shown in Figures 11a−c. The increase in temperature is due to the rate of heat generated by the reaction and rate of heat transmitted to the environment. The results show that the temperature at different depths is affected by the radiation intensity, initiator concentration, and the thickness as all three factors affect the rate of the reaction vs depth.

As seen in Table 1, comparing the runs shown in Figure 11b with Figure 11c, increasing the radiation intensity increases as expected the peak value of the temperature at the surface and near the bottom, since the rate at which heat produced is proportional to the cure rate/radiation intensity. Comparing the conditions for the run in Figure 11a with Figure 11c and the conditions for the run in Figure 11d with Figure 11e, the increase in temperature near the bottom of the sample is higher for the system with less photoinitiator. This is because the intensity with increasing depth is much lower for a system with higher initiator concentration. Table 1 also shows that the increase of the temperature near the bottom of the sample of CD540 with 0.05 wt % Irgacure 819. The temperature for the runs shown in Figures 11c,d is large, more than 25 °C. This is much higher than the temperature increase present in Figures 11a,b. In all of the systems the surface temperature does not increase much with initiator concentration as might be expected since the transfer of heat to the environment is much faster near the surface.

4.4. Applicability of the Model to Dimethacrylate and Other Thermosetting Systems. As discussed in section 3 under model description, it has been predicted and verified experimentally that dimethacrylate systems do form microgel regions and become spatially heterogeneous.[28,31−33,36,37] Numerous experimental results often using ESR measurements on a variety of dimethacrylate systems have shown that there are regions of high mobility, sometimes referred to as liquid-like monomer pools along with very low mobility regions in the growing microgel, macrogel regions where radicals are trapped making them essentially immobile.[21−26] Thus, we believe this model is widely applicable to dimethacrylate polymerizations. The older concepts involving more fitting parameters and free volume diffusion controlled k_p propagation and k_t termination rate constants are not a valid physical representation of these systems as they assume a spatial homogeneity. That is, they assume one can use the same k_p and k_t at a moment in time to describe the kinetics in both the mobile monomer pools and in the immobile gel regions. As such, the meaning of k_p and k_t is that they are an average of values which differ greatly with position in the heterogeneous space.

The applicability of the model to systems beyond dimethacrylates is dependent on the existence of the kinetics which cause a spatial heterogeneity. It has been suggested that many thermosets are inhomogeneous.[41] Heterogeneity is proposed to exist during free radical cross-linking polymerization of multifunctional monomers or by the step polymerization of three different monomers or the decrease in solubility of reaction products. The heterogeneity induced by these complex kinetics become fixed by the cross-linking. Hence, we would suggest that the model is viable in a variety of thermoset reactions which are more complex than step polymerization of two monomers.

5. Conclusions

UV cure kinetics in thick samples are functions of depth, incident radiation intensity, and strongly dependent initiator concentration. Increasing intensity will always increase the bulk cure rate, but increasing the initiator concentration can result in a decrease the bulk cure rate as the sample thickness increases.

A model which includes both bimolecular and unimolecular terminations arising from a changing concentration of mobile and trapped radicals describes accurately the cure kinetics at particular depths and the average cure kinetics through depth. The model's four kinetic parameters are based on thin film results and then models the thick system by dividing the sample into many thin layers (0.05 mm). The model predicted results show that the deeper the position in a thick film, the slower the cure rate. The model predictions and the experimental results also show that increasing the radiation intensity will always increase the bulk cure rate and shorten the inhibition period due to dissolved oxygen in thick samples. However, increasing the photoinitiator concentration may decrease the overall cure rate. The models predictions of cure at various depths describe how the radiation intensity and initiator concentration affect the cure as a function of depth in thick samples.

In summary, the model utilizes four fitting parameters, less than in several previously proposed models. More important, the advantage of the model is that the kinetic equation describing the kinetics in each layer vs depth and time is a more realistic physical representation of the spatial heterogeneity of the sample. That at each depth with time, the sample exhibits differing ratios of regions of high mobility and essentially no mobility

The bulk cure kinetics was monitored by transmitted real-time near-FTIR, and the results are in good agreement when compared to the corresponding predicted bulk UV cure vs time. The model, which does not include the temperature effect on the kinetics, does predict well the experimentally measured bulk cure kinetics of thick samples when the maximum temperature does not increase more than 15 °C. When the temperature increases more, the experimentally measured cure rate is in good agreement up to 40% conversion. But then due to the increasing temperature with depth, the experimentally measured rate of cure is faster, and the final conversion is higher than the model predictions as expected since the effect of temperature on the kinetics is not accounted for in the model.

References and Notes

(1) Lovell, L. G.; Berchtold, K. A.; Elliott, J. E.; Lu, H.; Bowman, C. N. *Polym. Adv. Technol.* **2001**, *12*, 335–345.
(2) Elliott, J. E.; Lovell, L. G.; Bowman, C. N. *Dent. Mater.* **2001**, *17*, 221–229.
(3) Lovell, L. G.; Stansbury, J. W.; Syrpes, D. C.; Bowman, C. N. *Macromolecules* **1999**, *32*, 3913–3921.
(4) Mueller, K. F.; Heiber, S. J. *J. Appl. Polym. Sci.* **1982**, *27*, 4043–4064.
(5) Schrof, W.; Beck, E.; Koniger, R.; Reich, W.; Schwalm, R. *Prog. Org. Coat.* **1999**, *35*, 197–204.
(6) Desilles, N.; Lecamp, L.; Lebaudy, P.; Bunel, C. *Polymer* **2003**, *44*, 6159–6167.
(7) Desilles, N.; Lecamp, L.; Lebaudy, P.; Bunel, C. *Polymer* **2004**, *45*, 1439–1446.
(8) Shen, M.; Bever, M. B. *J. Mater. Sci.* **1972**, *7*, 741.
(9) Martin, G. C.; Enssani, E.; Shen, M. *J. Appl. Polym. Sci.* **1981**, *26*, 1465–1473.
(10) Dror, M.; Elsabee, M. Z.; Berry, G. C. *J. Appl. Polym. Sci.* **1981**, *26*, 1741–1757.
(11) Xie, X. M.; Matsuoka, M.; Takemura, K. *Polymer* **1992**, *33*, 1996.
(12) Lee, J. H.; Prudhomme, R. K.; Aksay, I. A. *J. Mater. Res.* **2001**, *16*, 3536–3544.
(13) Decker, C.; Elzaouk, B. *J. Appl. Polym. Sci.* **1997**, *65*, 833–844.
(14) Decker, C. *Nucl. Instrum. Methods Phys. Res. B* **1999**, *151*, 22–28.
(15) Terrones, G.; Pearlstein, A. J. *Macromolecules* **2001**, *34*, 3195–3204.
(16) Terrones, G.; Pearlstein, A. J. *Macromolecules* **2001**, *34*, 8894–8906.
(17) O'Bren, A. K.; Bowman, C. N. *Macromolecules* **2003**, *36*, 7777–7782.
(18) Miller, G. A.; Gou, L.; Narayanan, V.; Scranton, A. B. *J. Polym. Sci., Part A: Polym. Chem.* **2002**, *40*, 793–808.
(19) Ivanov, V. V.; Decker, C. *Polym. Int.* **2001**, *50*, 113–118.
(20) Odian, G. *Principles Of Polymerization*, 3rd ed.; John Wiley & Sons: New York, 1991.
(21) Berchtold, K. A.; Randolph, T. W.; Bowman, C. N. *Macromolecules* **2005**, *38*, 6954–6964.
(22) Kloosterboer, J. G.; Lijten, C. M.; Greidanus, F. J. A. *Polymer* **1986**, *27*, 268–271.
(23) Kloosterboer, J. G.; Van de Hei, G. M. M.; Boots, H. M. J. *Polym. Commun.* **1984**, *25*, 354–357.

(24) Kloosterboer, J. G.; Van de Hei, G. M. M.; Gossink, R. G.; Dortant, G. C. M. *Polym. Commun.* **1984**, *25*, 322–325.
(25) Zhu, S.; Tian, Y.; Hamielec, A.; Eaton, D. R. *Polymer* **1990**, *31*, 1726–1734.
(26) Zhu, S.; Tian, Y.; Hamielec, A. E. *Macromolecules* **1990**, *23*, 1144–1150.
(27) Zhang, Y.; Kranbuehl, D.; Sautereau, H.; Seytre, G.; Dupuy, J. *Macromolecules* **2008**, *41*, 708–715.
(28) Rey, L.; Galy, J.; Sautereau, H. *Macromolecules* **2000**, *33*, 6780–6786.
(29) Terrones, G.; Pearlstein, A. J. *Macromolecules* **2004**, *37*, 1565–1575.
(30) Lecamp, L.; Lebaudy, P.; Youssef, B.; Bunel, C. *Polymer* **2001**, *42*, 8541–8547.
(31) Dusek, K. *Polym. Gels Networks* **1996**, *4*, 383–404.
(32) Dusek, K. *Angew. Makromol. Chem.* **1995**, *240*, 1–15.
(33) Dusek, K.; Matejka, L.; Spacek, P.; Winter, H. *Polymer* **1996**, *37*, 2233–2242.
(34) Berchtold, K. A.; Randolph, T. W.; Bowman, C. N. *Macromolecules* **2005**, *38*, 6954–6964.
(35) Anseth, K. S.; Anderson, K. J.; Bowman, C. N. *Macromol. Chem. Phys.* **1996**, *3*, 833–846.
(36) Guo, Z.; Sautereau, H.; Kranbuehl, D. E. *Polymer* **2005**, *46*, 12452–12459.
(37) Guo, Z.; Sautereau, H.; Kranbuehl, D. E. *Macromolecules* **2005**, *38*, 7992–7998.
(38) Jockusch, S.; Koptyug, I. V.; McGarry, P. F.; Sluggett, G. W.; Turro, N. J.; Watkins, D. M. *J. Am. Chem. Soc.* **1997**, *119*, 11495–11501.
(39) Jockusch, S.; Turro, N. J. *J. Am. Chem. Soc.* **1998**, *120*, 11773–11777.
(40) Cussler, E. L. *Diffusion-Mass Transfer in Fluid Systems*; Cambridge University Press: New York, 1984.
(41) Pascault, J. P., Sautereau, H.; Verdu, J.; Williams, R. J. J. *Thermosetting Polymers*; Marcel-Dekker: New York, 2002.

MA8019283